Accepted Manuscript

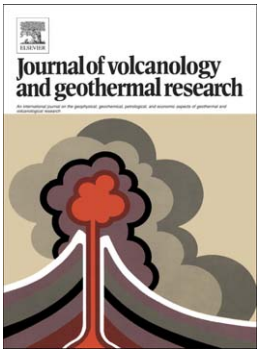

Fault plane orientations of microearthquakes at Mt. Etna from the inversion of P-wave rise times

Salvatore de Lorenzo, Elisabetta Giampiccolo, Carmen Martinez-Arevalo, Domenico Patanè, Annalisa Romeo

PII: S0377-0273(09)00443-0
DOI: doi: 10.1016/j.jvolgeores.2009.11.011
Reference: VOLGEO 4448

To appear in: *Journal of Volcanology and Geothermal Research*

Received date: 19 June 2009
Accepted date: 4 November 2009

Please cite this article as: de Lorenzo, Salvatore, Giampiccolo, Elisabetta, Martinez-Arevalo, Carmen, Patanè, Domenico, Romeo, Annalisa, Fault plane orientations of microearthquakes at Mt. Etna from the inversion of P-wave rise times, *Journal of Volcanology and Geothermal Research* (2009), doi: 10.1016/j.jvolgeores.2009.11.011

Fault plane orientations of microearthquakes at Mt. Etna from the inversion of P-wave rise times

Salvatore de Lorenzo

Dipartimento di Geologia e Geofisica & Centro Interdipartimentale per il Rischio Sismico e Vulcanico, Università di Bari, Italy

Elisabetta Giampiccolo

Istituto Nazionale di Geofisica e Vulcanologia, Sez. Di Catania, Italy

Carmen Martinez-Arevalo

Departamento de Volcanología, Museo Nacional de Ciencias Naturales, CSIC, Madrid (Spain)

Domenico Patanè

Istituto Nazionale di Geofisica e Vulcanologia, Sez. Di Catania, Italy

Annalisa Romeo

Dipartimento di Fisica, Università di Bari, Italy

Corresponding Author: *Salvatore de Lorenzo; telephone number: +39-080-5442619; fax number: +39-080-5442625, e-mail: delorenzo@geo.uniba.it*

Short Title: *fault plane orientations at Mt. Etna*

Abstract

A crucial point in the analysis of tectonic earthquakes occurring in a volcanic area is the inference of the orientation of the structures along which the ruptures occur. These structures represent zones of weakness which could favor the migration of melt toward the surface and the assessment of their geometry is a fundamental step toward efficient evaluation of volcanic risk. We analyzed a high-quality dataset of 171 low-magnitude, tectonic earthquakes occurred at Mt. Etna during the 2002-2003 eruption. We applied a recently developed technique aimed at inferring the source parameters (source size, dip and strike fault) and the intrinsic quality factor Q_p of P waves from the inversion of rise times. The technique is based on numerically calibrated relationships among the rise time of first P waves and the source parameters for a circular crack rupturing at a constant velocity. For the most of the events the directivity source effect did not allow us to constrain the fault plane orientation. For a subset of 45 events with well constrained focal mechanisms we were able to constrain the "true" fault plane orientation. The level of resolution of the fault planes was assessed through a non linear analysis based on the random deviates technique. The significance of the retrieved fault plane solutions and the fit of the assumed source model to data was assessed through a χ-square test. Most of the retrieved fault plane solutions agree with the geometrical trend of known surface faults. The inferred source parameters and Q_p are in agreement with the results of previous studies.

key words: rise time; circular crack model; nonlinear inversion; directivity

Introduction

The knowledge of the focal mechanism of an earthquake is a fundamental step for understanding geometry and dynamics of the seismogenic fault. Its determination is usually performed from the inversion of P-wave polarity (Reasenberg and Oppenheimer, 1985). Once the fault mechanism is computed, the next problem is deciding which of the two nodal planes corresponds to the true fault plane, except when the fault has clear surface morphological evidence which are confirmed by the hypocenter distribution at depth.

Several studies (Mori, 1996; de Lorenzo and Zollo, 2003; Filippucci et al., 2006; Warren and Shearer, 2006 among the others) have shown that the fault plane orientation of an earthquake can be inferred by modelling the directivity effect of the seismic source, i.e. the variation of the pulse widths of first P and/or S waves as a function of the angle between the normal to the fault plane and the seismic ray. However, the possibility to assess the "true" fault plane is strongly dependent on several factors such as the number of available data, the exploration of the range of takeoff angles, the error on the data and the ability of the theoretical source model to predict the data. Moreover, the equations governing the rise time variations with varying the model parameters are non linear. Therefore a statistical approach aimed at determining how data errors map onto the model parameter space is needed in order to assess the reliability of the results.

In this article, we present the results of a study aimed at inferring the fault plane orientation of events with well constrained focal mechanisms (Barberi et al., 2006) occurred at Mt. Etna during the 2002-2003 eruption. We used a recently developed pulse width technique (Filippucci et al., 2006) The source parameters of the events and the average intrinsic Q_p are also provided and compared with results of previous studies.

Tectonic setting

At Mt. Etna, signs of active tectonic processes are mainly recognised on the eastern flank of the volcano, as it is well demonstrated by the Timpe fault zone (Fig.1), which is characterized by both frequent shallow seismic activity and localized aseismic creep. The Timpe fault zone represents the northernmost prolongation of the NNW-SSE trending Malta Escarpment and is characterized by several individual faults with the same general strike of the escarpment. These fault segments are roughly parallel and of considerable length (8-10 km) with vertical offset (up to 200 m) that down-throw toward the sea.

It is worth noting that, while the Timpe faults mainly dominate the southern part of the eastern flank of Mt. Etna, other seismogenic structures, with predominantly ca. NE-SW Messina fault zone affinity, are recognisable in the northern part of the volcanic edifice (e.g., Lanzafame et al., 1996; and Azzaro, 1999). In fact, to the north the NNW-SSE fault system is interrupted by the E-W Pernicana fault, which cuts a large part of the volcanic edifice, and by the NE-SW Ripe della Naca system (Fig.1).

It is noteworthy that both the NNW-SSE and NE-SW structural trends are largely comparable to the main directions of the volcanic activity and the eruptive fractures on the upper flank of the volcano.

By a new detailed re-examination of historical sources and recent surface ruptures at Mt. Etna, Azzaro (1999) indicated that the kinematics of the two main seismogenic structures reported above is essentially associated with ruptures at shallow and very-shallow depth ($h < 1$ km). Moreover, the author suggested that the movements are consistent with a general ca. E-W extension expected in the sea-facing sector of the volcano, as also confirmed by fault plane solutions. Conversely, deeper earthquakes (hypocenter depths between 10 and 30 km) prevail in the western side under N-S oriented compressive

stresses, as suggested by several authors (e.g., Bonaccorso et al., 1996; Cocina et al., 1997; Patanè and Privitera, 2001).

The NNW-SSE trending structures are mainly characterised by quasi-pure normal dip-slip movements, with, therefore, a relevant extensional component. The NW-SE-trending structures, widely present in the eastern flank, show normal dip-slip displacements with minor dextral strike-slip movements. In addition, Azzaro (1999) indicated that in the southern medium-to-low slope flank, a semi-hidden 7 km long fault zone, consisting of three distinct recognisable segments, constitutes a blind seismogenic structure connecting the up-slope with the southern volcanic-rift zone. This should represent evidence of a continuous ca. N-S oriented tectonic system similar to that formed by the NE Rift.

Both NNW-SSE and NE-SW alignments are hypothesized as the main volcano-genetic structures (e.g., Bonaccorso et al., 1996; Gresta et al., 1998) which control the evolution of Mt. Etna, as their interference establishes a weakness volume along which magma can rise from depth (Rasà et al., 1995).

Small magnitude earthquakes generally precede, accompany and follow volcanic eruptions, contributing to the redistribution of the stress accumulated at the borders of the plumbing system.

Over the last 30 years Mt. Etna exhibited a high rate of eruptive events. In particular, the under study 2002-2003 flank eruption was accompanied by intense seismic activity. During the eruption, fracturing affected the south flank of the volcanic edifice along a N-S direction, the north flank along a direction nearly parallel to the NE Rift and some structural alignments on the southeast flank (Fig. 1).

Data selection

The data set is composed of 171 well located earthquakes (depth <5 km; $1.4<M_L<4.1$) (D'Amico and Maiolino, 2005), occurred at Mt. Etna between October 26, 2002 and December, 5, 2002 and recorded by the INGV network which, at that time, was composed by 24 velocity sensors having an instrumental response flat above 1 Hz (Fig.2). Although other stations were operating in the same period in the area, data at these stations exhibit either poor signal-to-noise ratio or saturated P waves, making them poor candidates for accurate P pulse analysis. The event localization (Fig.2) and ray tracing was performed in the 3D velocity model of the area (Patanè et al., 2006) using SIMULPS12 (Evans et al., 1994).

In a previous study it has been shown that the considered events have tectonic-earthquake-type waveforms, consistent with double-couple source mechanisms, with high-frequency content, sharp first arrivals, and clear P and S phases (Patane` and Giampiccolo, 2004). The P polarity reading and the inference of the focal mechanisms of these events have been previously performed (Barberi et al., 2006) using FPFIT (Reasenberg and Oppheneimer, 1985).

For each event, we measured the rise time τ of the first P wave at all the stations where the signal to noise ratio was sufficiently high to allow for the accurate individuation of the onset of first arrival P phase. We only used recordings for which the P phase picking has a time sample (0.01 s) accuracy. The rise time τ has been measured as the time interval between the onset of P wave and its first zero crossing time by accounting for the effect of noise *N* (Fig.3). Three measurements of the rise time compatible with the noise on data have been carried out. The first is based on the assumption that the onset of P wave has been rightly picked at the time T_0, which corresponds to a first zero crossing at the time T_1

and consequently to a rise time T_1-T_0. The other two measurements take into account the effect of noise. This is estimated, using the L1 norm, in a time window T_W= 0.5 s preceding the P wave onset, through the relation:

$$<|N|>=\frac{1}{T_W}\int_0^{T_W}|N(t)|dt$$

The intersections of the lines $v=\pm N$ with the ascending and descending ramps of the selected pulse allow to determine upper (T_{1B}-$T_{0\ B}$) and lower (T_{1A}-T_{0A}) bounds on the estimate of rise time (Fig.3). These three measurements of rise time allow the estimation of the average rise time and its error.

Since the measurement of τ requires only the first half cycle of the first P pulse it is the observable less sensitive to the complexities related to propagation effects. The waveforms showing clear multipathing effects during the first half cycle of first P wave (e.g. Deichmann, 1997; Filippucci et al., 2006) have been discarded. Clear multipathing effects are visible on the first half-cycle of the P wave as sharp discontinuities of the waveform (see for instance Fig. 10 in de Lorenzo and Zollo, 2003). However the effect of multipathing could be subtle, and this occurs when the secondary arrival adds in phase to the first P-wave arrival. To discard signals which could be affected by subtle multipathing effects, an accurate analysis based on the comparison between measurements of τ on velocity and squared velocity seismograms (Boatwright, 1984; de Lorenzo and Zollo, 2003) has been performed. In this way the signals for which the measurement of rise time on the squared velocity seismogram does not coincide, inside the error bound, with the measurement of rise time on velocity seismogram, have been discarded.

Based on previous resolution studies (de Lorenzo and Zollo, 2003; Filippucci et al., 2006) we discarded all the events for which a number of rise times less than six was available. After the data analysis only 143 of 171 events were available for the study.

Technique and data analysis

It is well known that the rise time of first P and/or S waves depends on both source and attenuation parameters (e.g. Boatwright, 1984). We used numerically calibrated relationships between the rise time and the source parameters and Q. These relationships are based on a kinematical model of seismic rupture (Zollo and de Lorenzo, 2001) and have been successively generalized to any crustal velocity model (de Lorenzo et al., 2004). If we assume that the seismic radiation is released by a circular crack rupturing at a constant velocity (Sato and Hirasawa, 1973), τ is related to the source dimension L, the rupture velocity c, the dip δ and strike ϕ of the fault, the takeoff angle θ and the quality factor Q_p through the relationship (de Lorenzo et al., 2004):

$$\tau = \tau_0 + \eta(L, c, \delta, \phi)\frac{T}{Q_P} + \lambda(L, c, \delta, \varphi) \qquad (1)$$

where:

$$\eta = \eta_1 \frac{L}{c}\sin\theta(\delta, \phi) + \eta_2 \qquad (2)$$

$$\lambda = \lambda_1 \frac{L}{c}\sin\theta(\delta, \phi) + \lambda_2 \qquad (3)$$

In equations (1)-(3) T is the source to receiver travel time and η_1, η_2, λ_1 and λ_2 are constants depending on the body wave velocity at the source. The values of these constants are tabulated in de Lorenzo et al. (2004) as a function of the body wave velocity.

The take off angle θ, the travel time T and their maximum errors have been computed in the 3D velocity model, using the relationships given in Zollo and de Lorenzo (2001) and accounting for the error on source localization and δ, ϕ computed by FPFIT in Barberi et al. (2006).

Using equation (1), for each fault plane retrieved from the inversion of P polarities (Barberi et al., 2006), the inversion of rise times is performed to estimate L and Q_p. The search of the best fit model parameter L and Q_p is performed through multiple runs of the Simplex Donwhill method (Press et al., 1989) in several subspaces of the whole admissible space of model parameters using random initializations of the initial simplex in each subspace. The details of the inversion technique are described in Zollo and de Lorenzo (2001). This allows us to predict, for each inverted model, the theoretical rise times τ_i^{teo} at each station. In this way the "true" fault plane is selected as that minimizing a L_2 norm misfit function σ between the observed τ_i^{obs} ($1<i\leq N$) and the theoretical rise times τ_i^{teo} ($1<i\leq N$) (Filippucci et al. 2006):

$$\sigma = \sqrt{\frac{\sum_{i=1}^{N}\left(\tau_i^{obs} - \tau_i^{teo}(\delta,\phi)\right)^2}{N-1}} \qquad (4)$$

where N is the number of rise times available for the event.

However, owing to the noise on data, we cannot be sure that the fault plane which minimizes (4) is the "true" fault plane. In fact, several sources of error can alter both the observed and the theoretical rise times. Whereas the noise in the seismic recordings is the cause of the error on the observed rise times, as discussed in the previous section, the error in source localization and the error on dip and strike as inferred from FPFIT map into an error in the takeoff angle which gives rise to an error in the theoretical rise time.

Therefore, to account for both the error on observed and theoretical rise times a statistical analysis based on the random deviates technique (Vasco and Johnson, 1998) has been performed. To this end, for each event, one-hundred inversions are carried out on one-hundred random datasets. Each dataset is built by adding to each datum a random quantity selected in its error range. If the misfit $\sigma(\delta_1,\phi_1)$ for a given fault plane orientation (δ_1,ϕ_1)

is systematically (i.e. in all the one-hundred inversions) smaller than the misfit $\sigma(\delta_2,\phi_2)$ for the other possible fault plane orientation (δ_2,ϕ_2), i.e. if the quantity:

$$\frac{\Delta\sigma}{\sigma(\delta_1,\phi_1)} = \frac{\sigma(\delta_2,\phi_2)-\sigma(\delta_1,\phi_1)}{\sigma(\delta_1,\phi_1)} \qquad (5)$$

is systematically greater than zero, then the selected fault plane is considered the possible "true" fault plane. Finally, for each event, the one-hundred estimates of L and Q_p are averaged to estimate the inverted parameters and their errors. If FPFIT does not provide multiple solutions, then, in equation (5), (δ_1,ϕ_1) is the plane which minimizes the standard deviation (the "true fault plane") and (δ_2,ϕ_2) is the auxiliary fault plane. If FPFIT provides multiple solutions then (δ_1,ϕ_1) and (δ_2,ϕ_2) are the two planes which give rise to the two smallest values of the misfit (equation (4)). Since these two planes do not necessarily belong to the same focal mechanism, the method allows to select both the most probable mechanism and the most probable fault plane orientation.

In Fig. 4, the quantity $\frac{\Delta\sigma}{\sigma(\delta_1,\phi_1)}$ is plotted as a function of the identification number of the one-hundred inversions, for one of the analyzed events. Since, for this event, $\frac{\Delta\sigma}{\sigma(\delta_1,\phi_1)}$ is systematically higher than zero (Fig.4), (δ_1,ϕ_1) is considered a possible "true fault plane". Fig. 5 shows the comparison among predicted and observed rise time vs. the takeoff angle for the same event.

After this analysis, a systematic standard deviation reduction was achieved only for 54 events (out of the initial 143), and therefore only these events were considered as potential "true" fault planes (Table I).

The next aspect we accounted for is the resolution of the fault plane estimates. It has been shown (de Lorenzo and Zollo, 2003; Filippucci et al., 2006) that the resolution depends in

a complex manner on several factors, such as the number and the error of data available in the inversion, the range of variation of the take off angles, the ability of the inverted model to fit the observed data and the misfit reduction from the auxiliary to the true fault plane. Moreover these factors are strictly correlated; as an example, a smaller sampling of the focal sphere could be compensated by a higher number of data used in the inversion and conversely. We quantified (Table I) the absolute level of resolution by using the parameter *R* (Filippucci et al., 2006):

$$R = N\frac{\Delta\theta}{(\pi/2)}\log_{10}\left[\frac{\Delta\sigma}{\sigma(\delta_1,\phi_1)}\frac{1}{\frac{\Delta\tau_{obs}}{\tau_{obs}}}\right] \qquad (6)$$

In equation (6) $\Delta\theta/(\pi/2)$ is the range of the takeoff angles covered by data normalized to the whole $\pi/2$ range and $\frac{\Delta\tau_{obs}}{\tau_{obs}}$ is the relative error on data. In Table I also the relative resolution R/R_{max} with respect to the best resolved fault plane is reported.

The above statistical analysis allowed us to select those earthquakes for which a preferential fault plane can be inferred from the two step inversion of P polarities and P rise times and also to quantify their relative resolution. Two open questions remain after this analysis. The first one is represented by the compatibility of the assumed circular crack source model with data and the second one is represented by the level of significance of the inferred solutions. These two aspects can be jointly assessed by carrying out a statistical test of hypothesis. In fact, if we assume that the errors on rise times are Gaussian distributed, the quantity:

$$\chi^2 = \sum_{i=1}^{N}\frac{(\tau_{i,obs}-\tau_{i,teo})^2}{(\Delta\tau_{i,obs})^2} \qquad (7)$$

will represent a χ^2 variable with a number of degrees of freedom equal to *N-k-1* where k = 2 is the number of parameters (L and Q_P) inferred from the inversion of rise times. Under this assumption, we can perform, in the dip-strike plane, a χ–square test for a given level of significance α (Cramèr, 1946) to accept or reject the null hypothesis H_0: (δ,ϕ) is the true fault plane orientation. If the solution retrieved from the inversion of rise times with the random deviates technique is confirmed from the χ^2 test, then the inferred fault plane is definitively accepted (Fig.6). This allows us to state that the considered source model is compatible with data and to quantify the level of significance of the solution. In Fig. 6 three examples are shown. In Fig. 6a the χ–square test allows us to constrain, with a level of significance α=25% the "true" fault plane of the event #1. In Fig. 6b the χ–square test indicates that the fault plane solution (δ=30°, ϕ=35°) inferred from the random deviates procedure has to be discarded at a level of significance α=25% in that other two fault planes (δ=90°, ϕ=30°), (δ=38°, ϕ=311°) lie in the region of acceptability of the test. In Fig. 6c the χ–square test indicates that the fault plane solution (δ=85°, ϕ=226°) inferred from the random deviates procedure can be accepted at a level of significance α=25% in that the other fault plane solutions do not lie in the region of acceptability of the test.

For each of the 54 above events, four chi-square tests were performed considering four levels of significance α (α=25,10,5,1 %). After this analysis, only for 45 events the χ-square tests confirmed the results of the inversion of rise times and only these events were considered as the true fault planes. These events and their level of significance are listed in Table II and the projection of the resolved planes on the Earth surface are plotted in Fig. 7 together with the focal mechanism solutions inferred from FPFIT (Barberi et al., 2006).

The average Q_P for the dataset was estimated using the relationship:

$$\langle Q_P \rangle = \frac{\sum_{i=1}^{Nev} w_i Q_i}{\sum_{i=1}^{Nev} w_i} \qquad (8)$$

where:

$$w_i = \frac{N_{ray}^i}{\Delta Q_i^2} \qquad (9)$$

In equation (9) N_{ray}^i is the number of rays available for the event i ($1 \leq i \leq N_{ev}$) and ΔQ_i the error on Q_i for the i-th event. We obtained $< Q_P >=42 \pm 10$ which agrees with a previous estimate of Q_P in the area (de Lorenzo et al., 2006).

The seismic moment M_0 was calculated from the local magnitude M_L (Table II) by using the relationship found by Giampiccolo et al. (2007):

$$Log(M_0) = (17.60 \pm 0.37) + (1.12 \pm 0.10) M_L \qquad (10)$$

Stress drop ($\Delta\sigma$) estimates were computed by using the Keilis-Borok (1959) scaling relationship:

$$\Delta\sigma = \frac{7}{16} \frac{M_0}{L^3} \qquad (11)$$

The estimated M_0 values were plotted vs. L in Fig. 8.

Discussion and conclusions

The present study marks an improvement in the knowledge of the faulting mechanism at Mt. Etna. The obtained results show that the directivity source effect on rise time can be very helpful to solve, at least for a subset of 45 events, the ambiguity between the true and the auxiliary fault plane of a focal mechanism (Table II; Fig.7). The majority of the inferred true fault planes (about 70%) strikes along a direction which is consistent with the trace of the main surface structures and eruptive fractures (pink thick lines in Fig.7). The remaining earthquakes (blue thick lines in Fig.7) do not match well with the strike of the

above mentioned fault systems. This result may be explained in terms of the complex evolution of Mt. Etna eruptive centers in a very long time interval (from 500 ky before present until today) (Tanguy et al., 1997) which results in the presence of strong heterogeneities of the subsurface rocks. Here, the high concentration of weakness zones with many orientations can act as preferential dislocation zones. In fact, the image of fault plane orientations revealed in this study is well different from the axial-symmetric ruptures which should occur in a homogeneous medium as the response to the stress acting during an eruption from a single eruptive center. Moreover, also the focal mechanisms of the whole data set of events selected in this study do not show preferential rupture alignments (Fig.9). Interestingly, a clear heterogeneity of the seismogenic stress and strain tensor in the area during the 2002-2003 eruption was previously inferred by several authors (Musumeci et al. 2004; Barberi et al.,2004; Barberi et al., 2006). Finally, a recent magnetotelluric study indicates a clear counter-clock rotation of about 45° of the strike of the Pernicana fault system from the surface to the bottom of the surface sedimentary cover (INGV 2004-2006 project report, A. Siniscalchi, personal communications).

The source dimensions of the resolved 45 events range between 100 and 500 m and stress drop of most of the events concentrated between 1 and 100 bars. Only few events have higher stress drop, up to 400 bars (Fig.8 and Table II). It is worth stressing that the present estimates of L (and therefore of $\Delta\sigma$) have to be considered dependent on the assumption of a fixed average rupture velocity V_r (V_r=0.9V_S) on which the theoretical eq. (1) has been built. This assumption could affect the retrieved source dimensions (de Lorenzo and Zollo, 2003). However, despite this limitation, the obtained source parameters and scaling laws are consistent with those obtained by Giampiccolo et al. (2007) from the analysis of the same data set in the frequency domain and outline a characteristic of the region. In fact we

deduce a general agreement of the present source parameter and Q_p estimates at Mt. Etna with those inferred from the use of different techniques and different source models (de Lorenzo et al., 2006; Giampiccolo et al., 2007).

In conclusion, the variety of the fault plane solutions and the small values of L and $\Delta\sigma$ indicate the presence of planes of weakness with different orientations to accommodate the slip, which could represent low-strength structures where great stress accumulation is hindered.

Figure captions

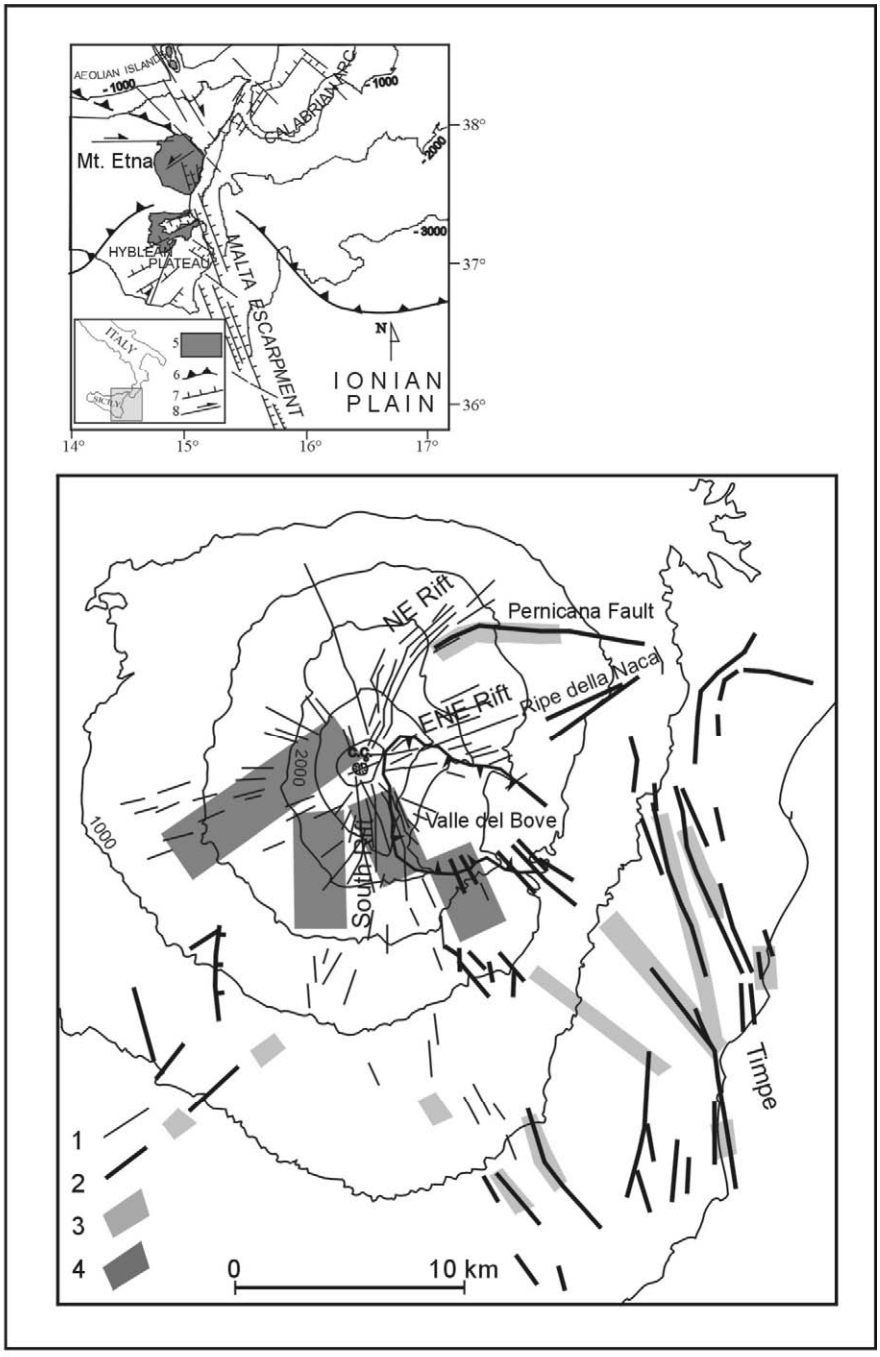

Fig.1

Fig.1. Structural map of Mt. Etna (after Azzaro et al., 1999). 1. eruptive fractures; 2. main faults; 3. coseismic surface faulting zones; 4. zones where seismicity is mainly clusterized.

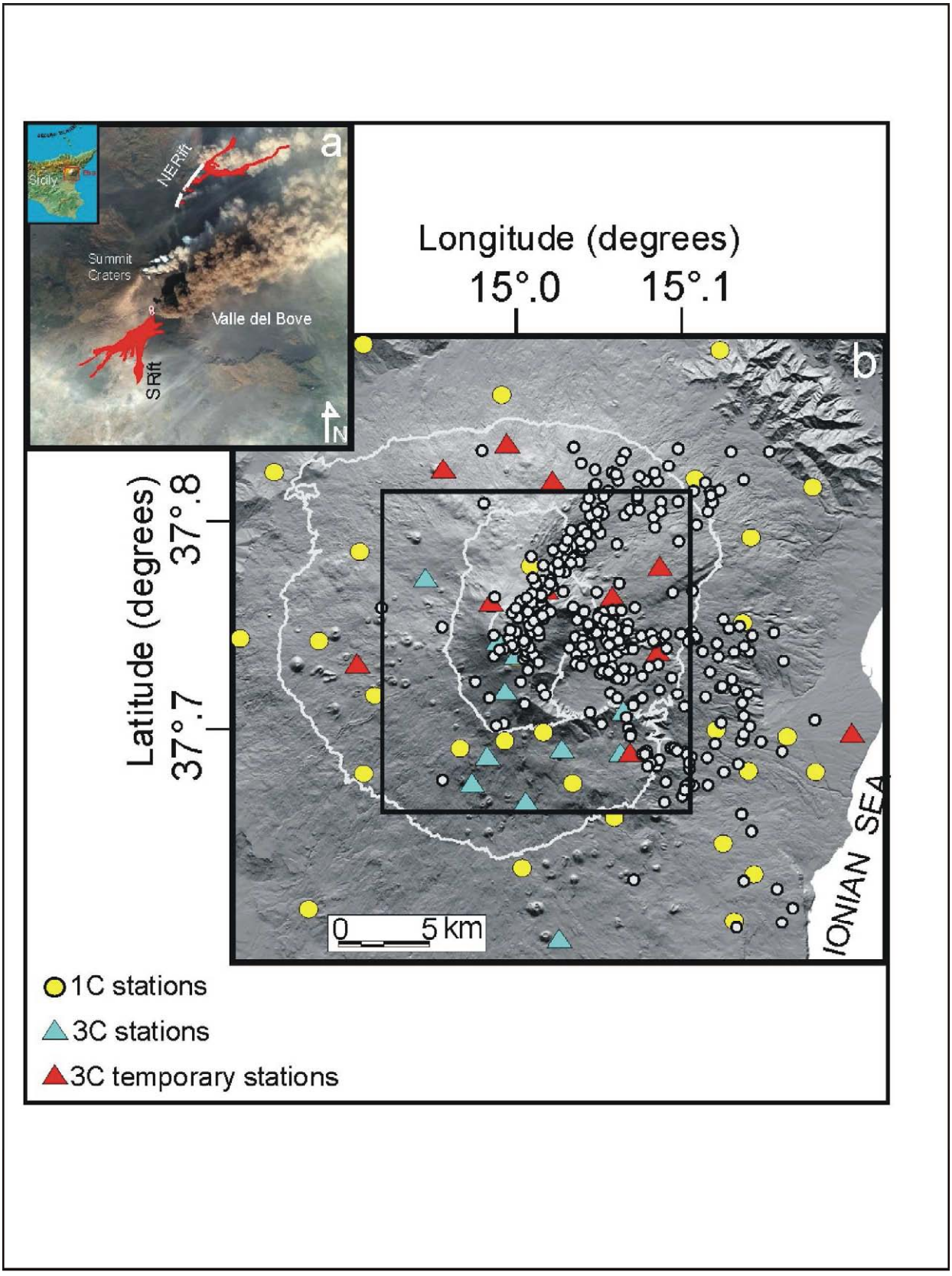

Fig. 2

Fig.2. Epicenters (circles) of the earthquakes occurred during the 2002-2003 Mt. Etna eruption considered in this study and seismic stations distribution (triangles).

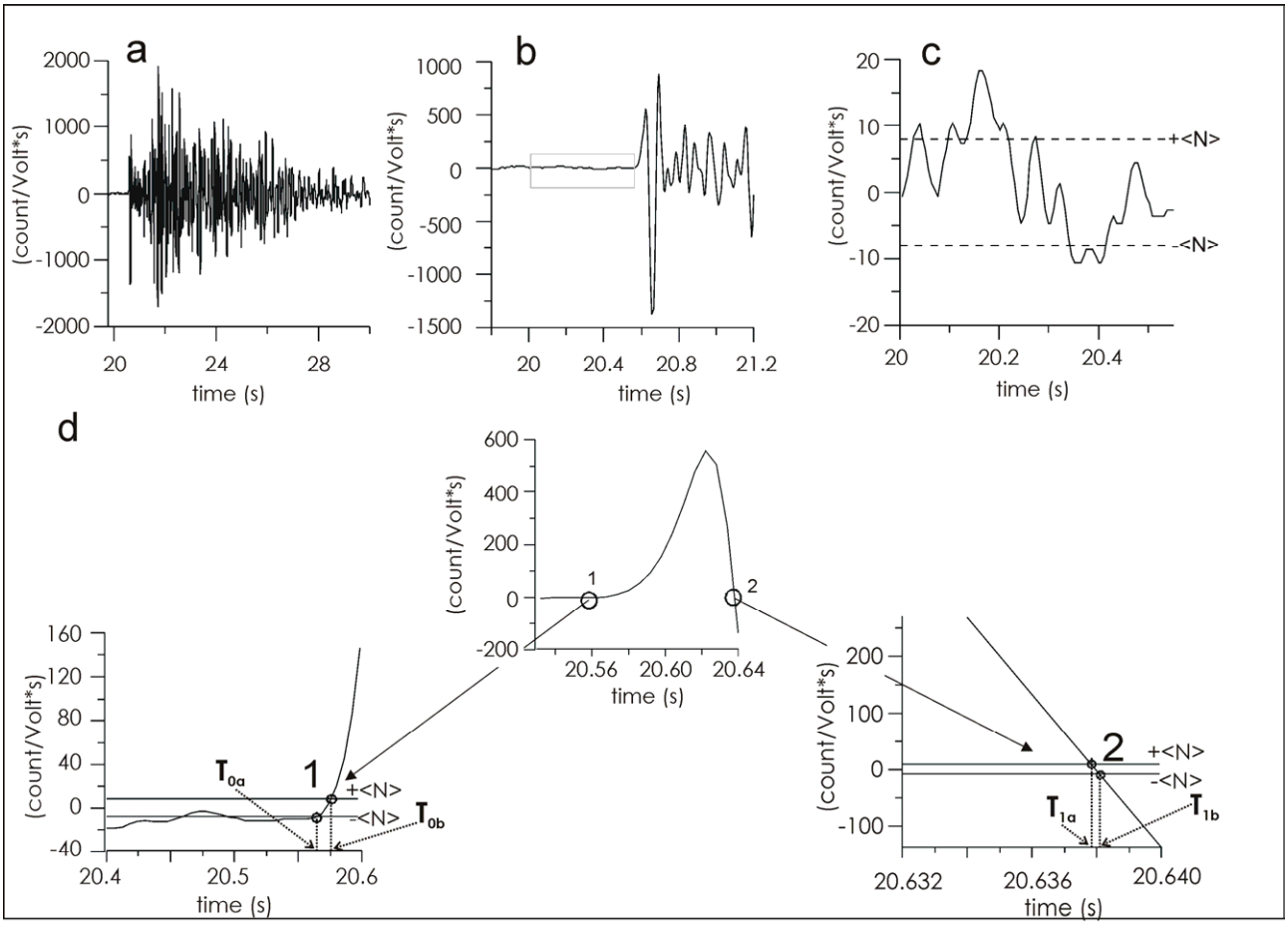

Fig.3

Fig.3. Measurement of rise time on a velocity seismogram (a) recorded at Mt. Etna. On the top, the time window (b) preceding the P wave onset used to quantify the error in L_1 norm (c) and its effect (d) on the estimates of the first P wave arrival (T_{0a},T_{0b}) and on the first zero crossing time (T_{1a},T_{1b}).

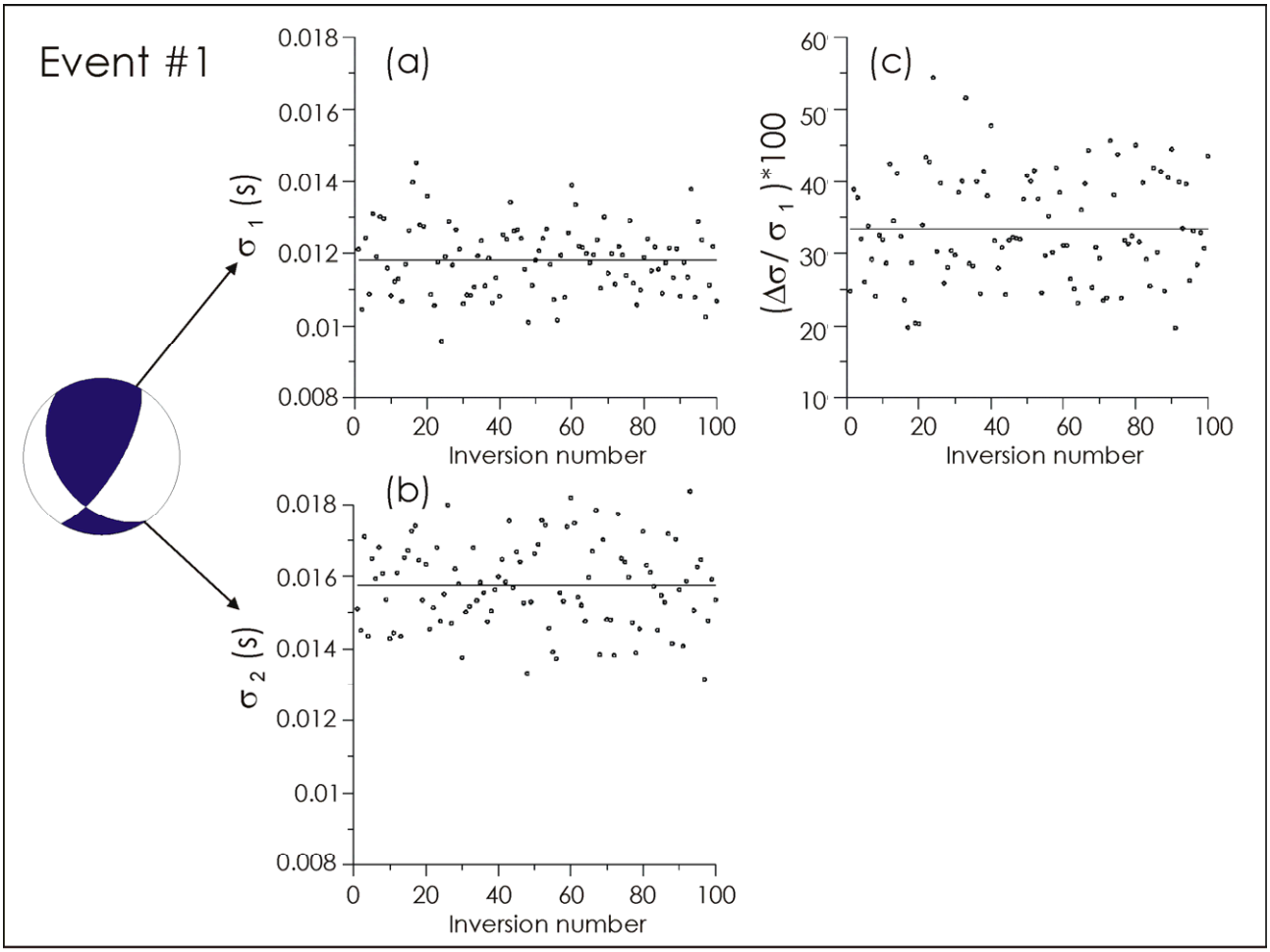

Fig.4

Fig.4. Plot of the standard deviation vs. the inversion number in the random deviates approach for an event considered in this study. Since the standard deviation (a) for the fault plane (δ_1,ϕ_1) is systematically smaller than the standard deviation (b) for the fault plane (δ_2,ϕ_2) a systematic standard deviation occurs (c) indicating that fault plane 1 is a possible true fault plane.

Fig.5

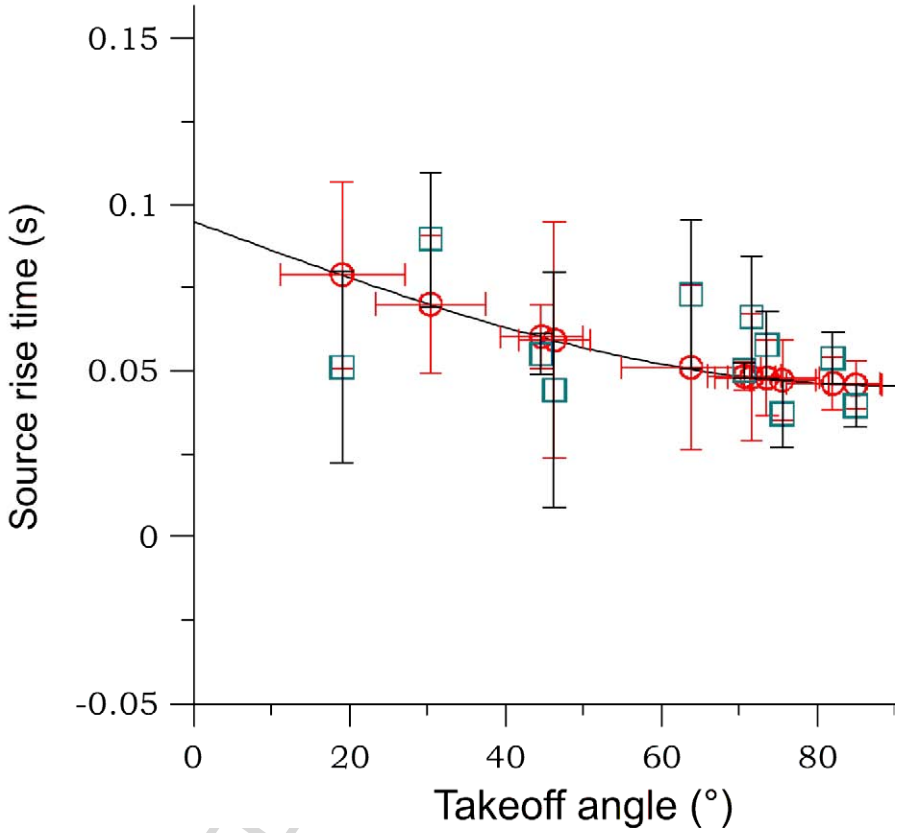

Fig.5. Comparison among observed (blue squares) and predicted (red circles) source rise times and their errors vs. the takeoff angle for the event #1.

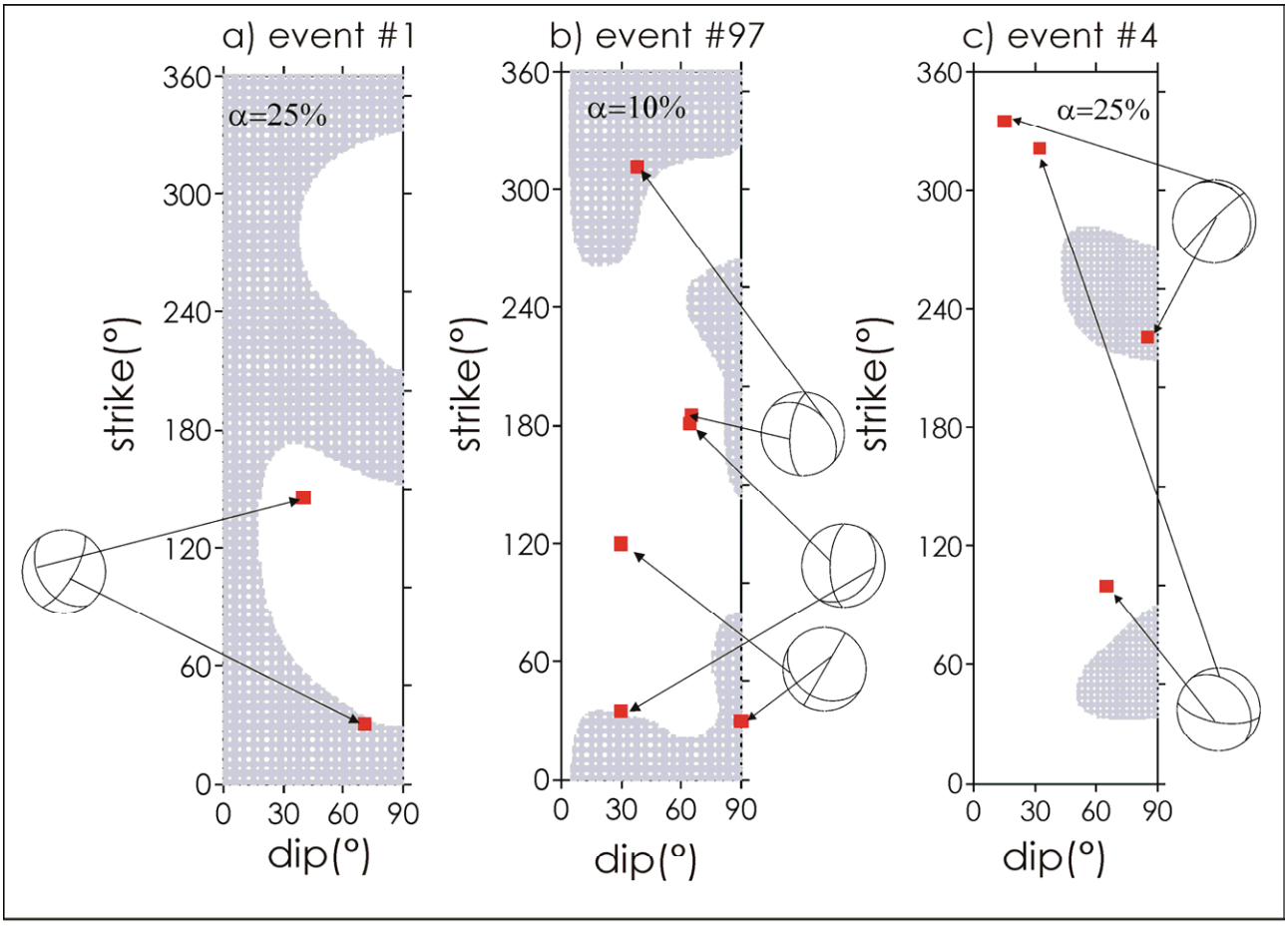

Fig.6

Fig.6. Chi-square tests for three considered events. The grey areas represent regions of acceptability of the solutions and the red squares the solutions inferred from FPFIT. In (a) it is shown the case of a test which confirms the null hypothesis (see the text). In (b) it is shown the case of a test which does not confirm the null hypothesis for a multiple FPFIT solution. In (c) it is shown the case of a test which confirm the null hypothesis for a multiple FPFIT solution.

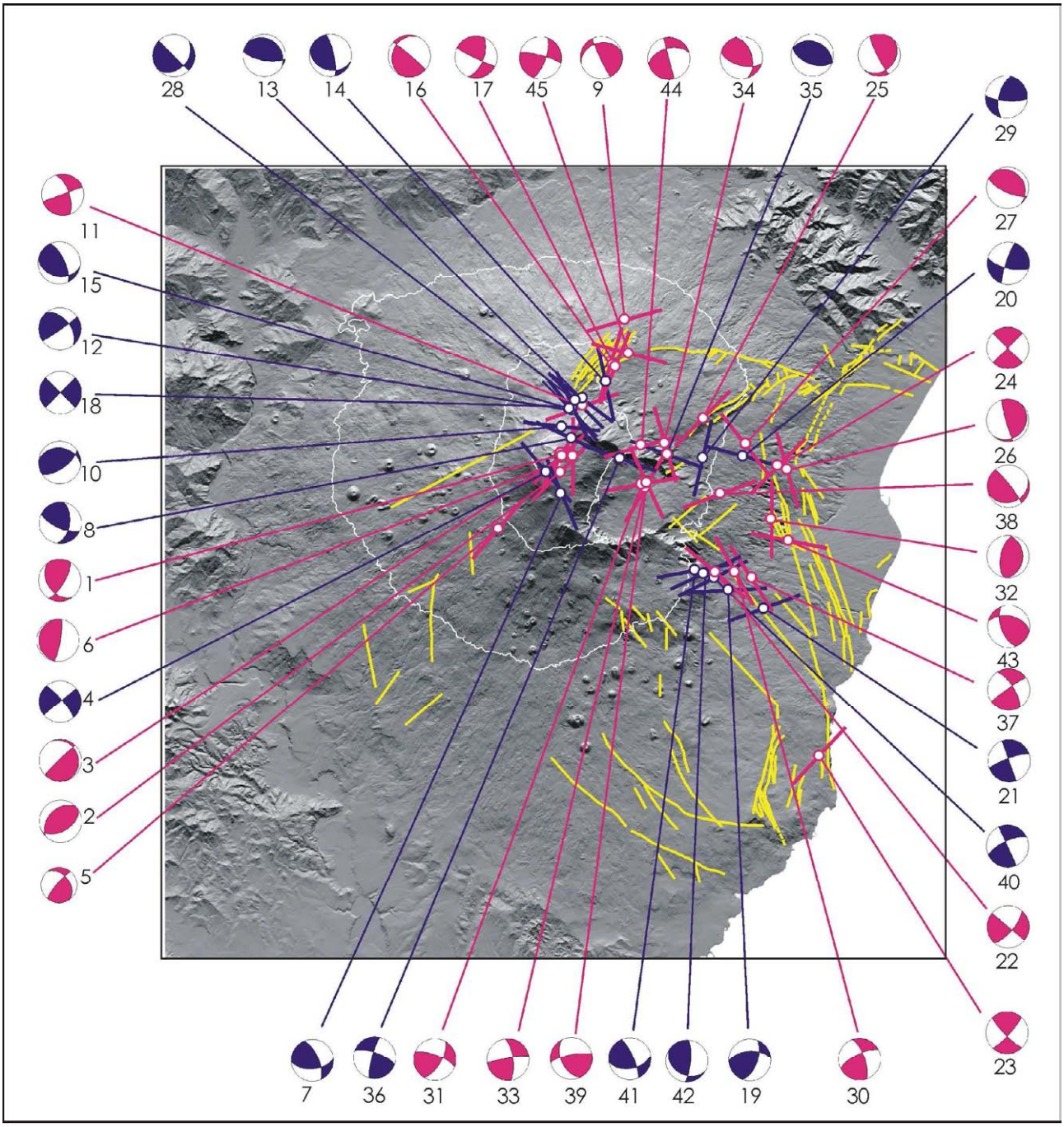

Fig.7

Fig.7. Map showing the surface projections (pink and blue lines) and the focal mechanisms of the 45 retrieved faults planes. The main structures (yellow lines) are also reported (after Azzaro, 1999). Pink segments indicate solutions in agreement with known structures; blue segments indicate solutions not directly correlated with surface geology.

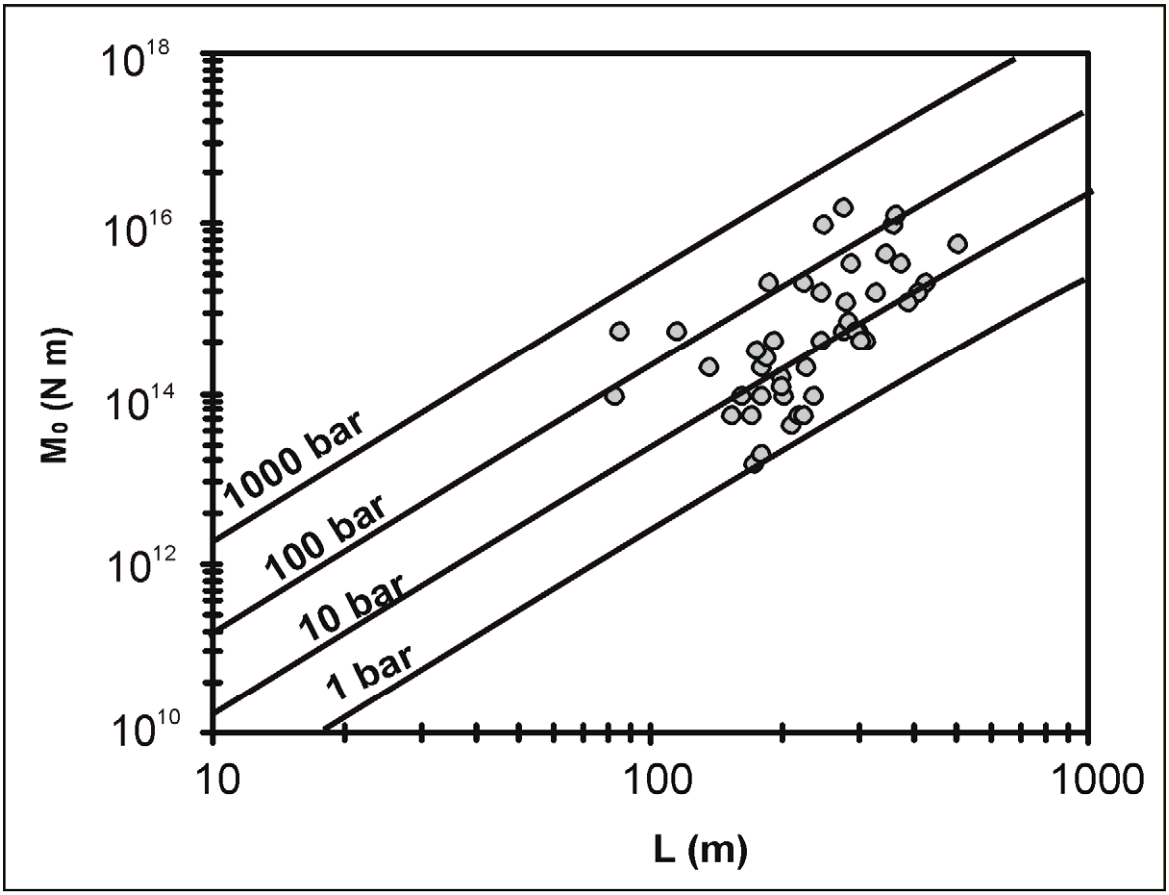

Fig.8

Fig.8. Relationship between seismic moment and source radius for the earthquake listed in Table II. The lines of constant stress drop are also reported.

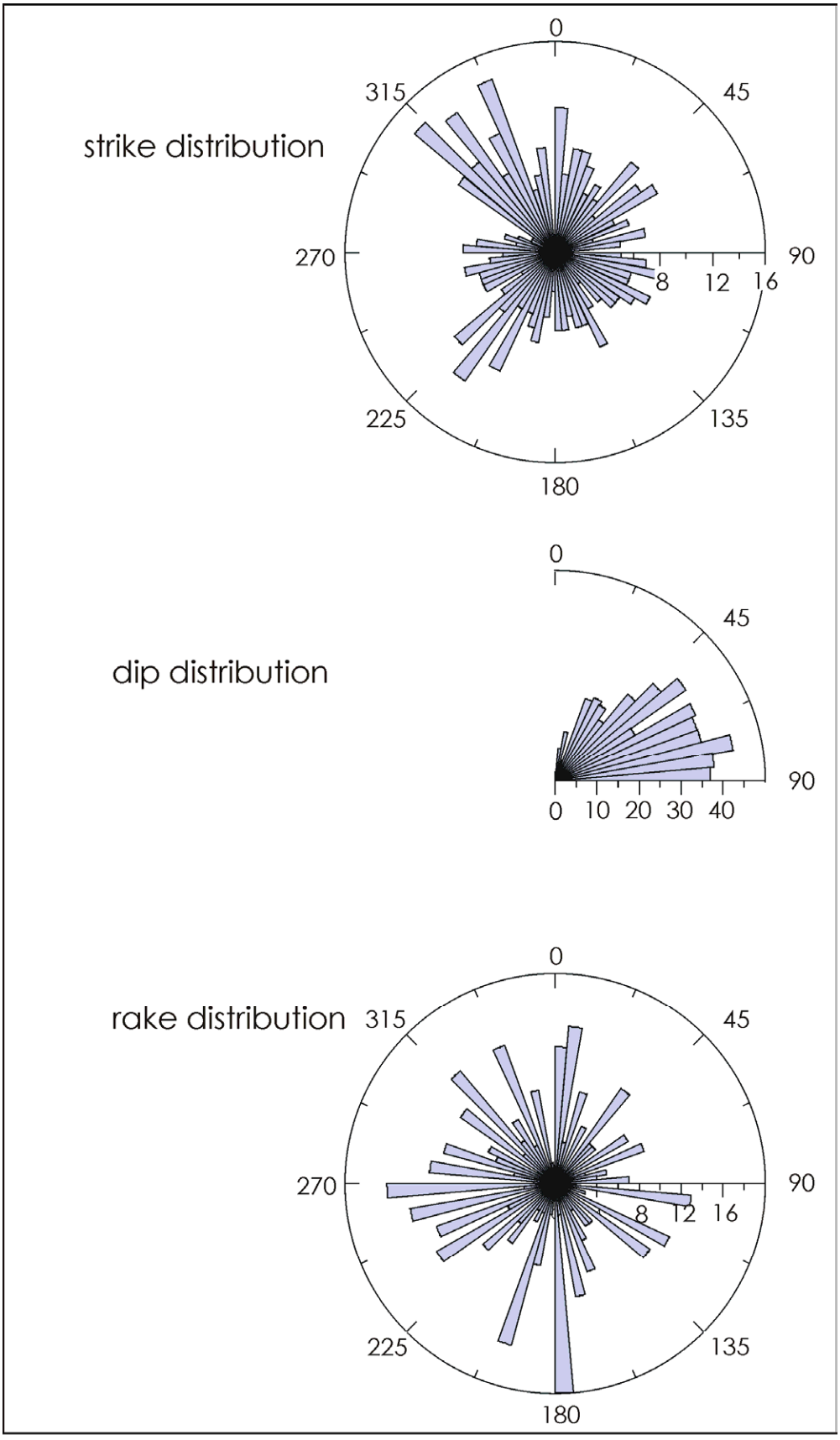

Fig.9

Fig.9. Rose diagrams showing the distribution of strike dip and rake inferred from FPFIT for the whole data set of 143 events.

Table captions

Table I. Results of the inversion of P rise times for 54 events and relative errors. In bold the retrieved "true" fault planes.

								FPFIT			FPFIT									
#	Date	hh:mm	Lat.N	Long.E	Depth	Gap	M_L	ϕ_1	δ_1	λ_1	ϕ_2	δ_2	λ_2	$100\frac{\Delta\sigma}{\sigma(\delta_1,\phi_1)}$	n_data	$100\frac{\Delta\tau_{obs}}{\tau_{obs}}$	$\Delta\theta/(\pi/2)$	R	R/Rmax	L(m)	ΔL(m)
1	20021026	21.35	37.755	15.003	-0.72	54	1.8	145	40	-150	**31**	**71**	**-54**	24.8	11	12.5	0.36	1.17	0.15	212	12
2	20021026	21.55	37.742	15.000	0.05	50	1.6	85	50	40	**327**	**61**	**132**	30.4	7	6.7	0.96	4.41	0.58	118	12
3	20021026	22.28	37.746	15.002	0.07	52	1.9	60	50	100	**225**	**41**	**78**	43.9	11	7.8	0.93	7.67	1.00	220	15
4	20021027	0.21	37.754	15.003	-0.12	87	2.1	335	15	-160	**226**	**85**	**-76**	10	6	9.1	0.84	0.21	0.03	83	18
5	20021027	0.3	37.746	14.993	-1.10	54	2.8	50	90	10	**320**	**80**	**180**	12.7	6	5.0	0.76	1.86	0.24	86	35
6	20021027	0.35	37.717	14.962	2.15	73	3.3	**220**	**80**	**130**	322	41	15	38.2	6	14.7	0.70	1.74	0.23	226	20
7	20021027	0.36	37.754	15.010	-0.41	56	2.4	**180**	**10**	**80**	10	80	92	44.4	9	12.1	0.17	0.84	0.11	229	15
8	20021027	0.41	37.735	15.003	-1.70	41	3.9	85	55	-150	**337**	**66**	**-39**	26.9	6	17.8	0.73	0.79	0.10	250	35
9	20021027	1.11	37.763	15.009	-0.91	47	3.5	**115**	**70**	**-140**	9	53	-25	22.7	7	5.0	0.60	2.75	0.36	374	147
10	20021027	1.28	37.823	15.043	-0.71	88	4.1	155	85	120	**254**	**30**	**10**	15.6	6	5.0	0.29	0.86	0.11	276	24
11	20021027	1.42	37.769	15.003	-1.39	67	3.3	55	65	70	**276**	**32**	**126**	8.7	6	5.0	0.41	0.59	0.08	187	33
12	20021027	2.18	37.779	15.016	-1.71	118	3.9	340	65	-180	**250**	**90**	**-25**	40.7	8	14.1	0.96	3.52	0.46	360	47
13	20021027	2.29	37.777	15.010	0.05	121	4.0	55	85	40	**321**	**50**	**173**	17.2	6	8.3	0.92	1.76	0.23	367	51
14	20021027	2.42	37.825	15.086	-1.69	115	4.2	45	65	0	**315**	**90**	**155**	29.4	6	17.2	0.38	0.53	0.07	447	39
15	20021027	3.28	37.783	15.016	-1.65	138	3.5	100	70	80	**307**	**22**	**116**	14.4	6	13.0	0.36	0.10	0.01	289	28
16	20021027	5.2	37.791	15.031	-1.95	131	3.2	105	30	30	**348**	**76**	**117**	22	7	11.4	0.68	1.36	0.18	247	10
17	20021027	6.26	37.779	15.010	0.23	162	3.3	100	35	40	**335**	**68**	**118**	27.8	6	8.9	0.98	2.91	0.38	428	13
18	20021027	6.49	37.787	15.023	1.01	143	3.8	**25**	**75**	**-40**	127	52	-161	9	6	7.6	0.64	0.28	0.04	450	31
19	20021027	12.09	37.795	15.035	-0.77	82	2.9	**310**	**90**	**40**	220	50	180	10	6	9.4	0.55	0.09	0.01	281	20
20	20021027	14.42	37.800	15.039	-0.30	89	3.1	310	85	70	**207**	**21**	**166**	9	6	8.4	0.12	0.02	0.00	413	30
21	20021027	16.02	37.799	15.037	-0.65	92	3.2	115	85	30	**22**	**60**	**174**	50.3	6	9.1	0.48	2.16	0.28	411	15
22	20021028	3.01	37.812	15.040	-2.03	76	4.0	**160**	**50**	**130**	287	54	53	.15	6	5.0	0.14	0.40	0.05	227	15
23	20021028	16.27	37.778	15.008	-0.39	43	3.2	**315**	**90**	**180**	45	90	0	18.6	13	9.3	0.50	1.96	0.26	329	18
24	20021029	1.31	37.686	15.109	0.26	124	2.7	20	60	40	**267**	**56**	**143**	9	9	8.4	0.90	0.25	0.03	246	11
25	20021029	9.13	37.681	15.123	1.84	116	2.8	70	65	20	**331**	**72**	**154**	28.2	8	11.0	0.71	2.31	0.30	295	11
26	20021029	10.02	37.754	15.119	6.17	47	2.8	**105**	**70**	**-10**	198	81	-160	8.3	9	7.4	0.82	0.37	0.05	300	62
27	20021029	10.04	37.677	15.132	1.32	116	3.1	340	90	-170	**250**	**80**	**0**	15.5	12	7.5	0.95	3.56	0.46	391	22
28	20021029	10.13	37.695	15.101	-0.24	88	2.8	40	70	0	**310**	**90**	**160**	8.2	6	7.8	0.88	0.11	0.01	116	26
29	20021030	10.47	37.602	15.167	2.54	156	2.4	135	80	10	**43**	**80**	**170**	23.7	6	15.2	0.28	0.32	0.04	181	10
30	20021030	15.25	37.810	15.113	0.96	76	3.3	120	30	-180	**30**	**90**	**-60**	27.8	6	12.6	0.98	2.03	0.27	220	17
31	20021031	6.4	37.749	15.141	4.17	165	2.1	315	90	0	**225**	**90**	**180**	17.4	6	5.0	0.58	1.88	0.25	238	10

32	20021031	7.34	37.773	15.093	4.33	151	1.9	**45**	**25**	**-20**	153	82	-114	59.7	6	11.0	0.95	4.18	0.54	171	10
33	20021031	10.41	37.747	15.147	5.39	136	2.8	45	15	-30	**164**	**83**	**-103**	22.2	11	9.1	0.84	3.55	0.46	276	20
34	20021031	20.02	37.760	15.120	5.10	145	1.9	115	70	-100	**322**	**22**	**-64**	27.3	6	9.3	0.90	2.53	0.33	153	22
35	20021101	6.38	37.724	15.133	4.9	152	2.1	**40**	**40**	**-90**	220	50	-90	16.3	6	6.3	0.89	2.19	0.29	157	10
36	20021101	15.32	37.782	15.012	-0.68	43	2.9	45	35	0	**315**	**90**	**125**	51.7	6	16.1	0.76	2.31	0.30	284	16
37	20021102	10.33	37.753	15.093	3.68	123	1.4	95	75	-30	**193**	**61**	**-163**	27.7	6	8.1	0.17	0.54	0.07	173	7
38	20021102	17.09	37.695	15.114	2.54	147	2.3	340	70	-160	**243**	**71**	**-21**	12.3	12	9.5	0.71	0.94	0.12	199	19
39	20021102	23.08	37.738	15.056	2.82	68	2.4	**30**	**65**	**20**	291	72	154	12.4	15	9.2	0.74	1.44	0.19	136	8
40	20021103	0.22	37.722	15.137	4.93	169	2.1	**0**	**30**	**-100**	192	61	-84	22.5	6	5.8	0.79	2.80	0.36	179	8
41	20021103	5.36	37.740	15.054	1.90	69	2.1	**260**	**85**	**160**	352	70	5	18.1	7	13.9	0.31	0.25	0.03	202	31
42	20021104	10.52	37.760	15.069	1.57	82	2.7	105	60	-130	**344**	**48**	**-42**	26.5	12	7.1	0.52	3.57	0.47	312	14
43	20021104	12.21	37.755	15.070	1.54	103	1.5	**110**	**55**	**-90**	290	35	-90	51.5	6	8.2	0.35	1.69	0.22	179	14
44	20021107	6.16	37.753	15.040	1.59	52	2.7	195	80	-20	**289**	**70**	**-169**	8.4	10	7.3	0.90	0.55	0.07	192	11
45	20021107	9.03	37.692	15.124	-0.04	182	1.9	235	85	-20	**327**	**70**	**-175**	46.5	6	6.2	0.29	1.52	0.20	224	21
46	20021107	15.07	37.735	15.104	5.06	140	2.1	**70**	**25**	**-160**	322	82	-66	57.3	6	8.4	0.76	3.82	0.50	162	11
47	20021117	9.26	37.741	15.057	1.81	71	2.8	**155**	**50**	**-20**	258	75	-138	25.3	12	6.0	0.39	2.96	0.39	296	13
48	20021124	6.59	37.692	15.100	4.09	99	3.7	335	90	20	**245**	**70**	**180**	6.5	8	5.0	0.43	0.39	0.05	507	18
49	20021124	10.27	37.696	15.088	4.45	110	2.5	**80**	**50**	**-160**	337	75	-42	34.8	9	5.0	0.99	7.49	0.98	186	10
50	20021124	11.03	37.694	15.092	4.59	73	2.9	**90**	**60**	**20**	350	73	148	9.7	12	6.0	0.99	2.47	0.32	125	7
51	20021124	13.56	37.694	15.093	4.33	117	2.6	5	75	120	**119**	**33**	**28**	14.1	10	7.0	0.53	1.62	0.21	176	15
52	20021202	12.28	37.711	15.148	-1.83	169	3.6	160	60	-50	**281**	**48**	**-138**	29.8	6	5.0	0.54	2.49	0.32	345	10
53	20021205	0.4	37.759	15.054	-1.01	84	2.2	345	90	40	**255**	**50**	**180**	31.4	7	5.0	0.22	1.24	0.16	201	7
54	20021205	22.59	37.806	15.046	-1.27	103	2.7	**285**	**80**	**-20**	19	70	-169	24.7	6	5.0	0.43	1.78	0.23	305	33

Table II. Focal parameters and relative errors as inferred from FPFIT for the 45 events accepted after the χ-square test. The misfit function F of the focal mechanism solutions, as inferred from FPFIT, is also reported.

#	Str1	Dip1	Rake1	Str2	Dip2	Rake2	F	ΔStr	ΔDip	ΔRake	ΔStr	M_L	L(m)	ΔL	M_0(N m)	Δσ (bar)	α(%)
1	145	40	-150	**31**	**71**	**-54**	0.11	10	5	10	10	1.8	212	12	4.13E+13	1.90	25
3	60	50	100	**225**	**41**	**78**	0.07	3	10	5	3	1.9	220	15	5.35E+13	2.20	10
4	335	15	-160	**226**	**85**	**-76**	0.04	20	5	20	20	2.1	83	18	8.95E+13	68.51	25
5	50	90	10	**320**	**80**	**180**	0.03	5	15	10	5	2.8	86	35	5.45E+14	374.53	5
6	**220**	**80**	**130**	322	41	15	0.10	5	5	20	5	3.3	226	20	1.98E+15	74.93	25
7	**180**	**10**	**80**	10	80	92	0.05	10	0	10	10	2.4	229	15	1.94E+14	7.07	25
8	85	55	-150	**337**	**66**	**-39**	0.12	3	8	5	3	3.9	250	35	9.29E+15	260.11	25
9	**115**	**70**	**-140**	9	53	-25	0.18	3	3	0	3	3.5	374	147	3.31E+15	27.69	1
10	155	85	120	**254**	**30**	**10**	0.02	10	13	20	10	4.1	276	24	1.56E+16	323.78	25
11	55	65	70	**276**	**32**	**126**	0.07	3	10	5	3	3.3	187	33	1.98E+15	132.27	5
12	340	65	-180	**250**	**90**	**-25**	0.01	10	13	20	10	3.9	360	47	9.29E+15	87.11	25
13	55	85	40	**321**	**50**	**173**	0.04	3	10	10	3	4.0	367	51	1.20E+16	106.41	1
15	100	70	80	**307**	**22**	**116**	0.05	8	5	0	8	3.5	289	28	3.31E+15	60.02	10
16	105	30	30	**348**	**76**	**117**	0.20	10	0	40	10	3.2	247	10	1.53E+15	44.35	10
17	100	35	40	**335**	**68**	**118**	0.12	20	3	10	20	3.3	428	13	1.98E+15	11.03	25
19	**310**	**85**	**70**	207	21	166	0.00	8	8	10	8	3.1	281	20	1.18E+15	23.27	25
21	115	85	30	**22**	**60**	**174**	0.10	8	13	5	8	3.2	411	15	1.53E+15	9.63	5
23	**315**	**90**	**180**	45	90	0	0.03	3	13	5	3	3.2	329	18	1.53E+15	18.77	25
24	20	60	40	**267**	**56**	**143**	0.11	5	8	10	5	2.7	246	11	4.21E+14	12.36	25
26	**105**	**70**	**-10**	198	81	-160	0.06	10	18	5	10	2.8	300	62	5.45E+14	8.82	5
27	340	90	-170	**250**	**80**	**0**	0.01	0	0	15	0	3.1	391	22	1.18E+15	8.64	5
28	40	70	0	**310**	**90**	**160**	0.07	18	45	30	18	2.8	116	26	5.45E+14	152.62	25
29	135	80	10	**43**	**80**	**170**	0.00	3	10	70	3	2.4	181	10	1.94E+14	14.32	5
31	315	90	0	**225**	**90**	**180**	0.10	3	10	10	3	2.1	238	10	8.95E+13	2.91	1
32	**45**	**25**	**-20**	153	82	-114	0.00	30	8	20	30	1.9	171	10	5.35E+13	4.68	25
33	45	15	-30	**164**	**83**	**-103**	0.05	5	3	5	5	2.8	276	20	5.45E+14	11.33	10
34	115	70	-100	**322**	**22**	**-64**	0.00	10	0	20	10	1.9	153	22	5.35E+13	6.53	5
36	45	35	0	**315**	**90**	**125**	0.12	8	8	10	8	2.9	284	16	7.05E+14	13.46	25
37	95	75	-30	**193**	**61**	**-163**	0.06	10	5	25	10	1.4	173	7	1.47E+13	1.24	25
38	340	70	-160	**243**	**71**	**-21**	0.07	10	20	10	10	2.3	199	19	1.50E+14	8.33	5
39	**30**	**65**	**20**	291	72	154	0.10	5	10	15	5	2.4	136	8	1.94E+14	33.76	5
40	**0**	**30**	**-100**	192	61	-84	0.11	8	0	5	8	2.1	179	8	8.95E+13	6.83	5
41	**260**	**85**	**160**	352	70	5	0.12	0	8	25	0	2.1	202	31	8.95E+13	4.75	25
42	105	60	-130	**344**	**48**	**-42**	0.08	10	10	5	10	2.7	312	14	4.21E+14	6.06	10
43	**110**	**55**	**-90**	290	35	-90	0.00	50	15	25	50	1.5	179	14	1.91E+13	1.45	10
44	195	80	-20	**289**	**70**	**-169**	0.09	3	18	30	3	2.7	192	11	4.21E+14	26.01	1
45	235	85	-20	**327**	**70**	**-175**	0.00	10	13	10	10	1.9	224	21	5.35E+13	2.08	5

46	**70**	**25**	**-160**	322	82	-66	0.00	15	5	10	15	2.1	162	11	8.95E+13	9.21	10
47	**155**	**50**	**-20**	258	75	-138	0.06	5	3	20	5	2.8	296	13	5.45E+14	9.19	10
48	335	90	20	**245**	**70**	**180**	0.12	13	10	10	13	3.7	507	18	5.55E+15	18.62	1
49	**80**	**50**	**-160**	337	75	-42	0.13	3	3	0	3	2.5	186	10	2.51E+14	17.08	5
51	**5**	**75**	**120**	119	33	28	0.00	3	8	5	3	2.6	176	15	3.25E+14	26.09	5
52	160	60	-50	**281**	**48**	**-138**	0.11	8	13	20	8	3.6	345	10	4.29E+15	45.66	25
53	345	90	40	**255**	**50**	**180**	0.07	5	5	5	5	2.2	201	7	1.16E+14	6.24	10
54	**285**	**80**	**-20**	19	70	-169	0.14	8	20	5	8	2.7	305	33	4.21E+14	6.49	5

Acknowledgements: The authors thank Gilberto Saccorotti and an anonymous reviewer for their valuable comments which improved the manuscript. P. Dellino and A. Siniscalchi are acknowledged for their useful suggestions. Many thanks to Ann Brown for the corrections to the English text.

References

Azzaro, R. (1999), Earthquake surface faulting at Mt. Etna volcano (Sicily) and implications for active tectonics, *J. Geodyn.*, **28**, 193 – 213, doi:10.1016/S0264-3707(98)00037-4.

Barberi, G., Cocina, O., Patanè, D., 2006. Fast deformation processes at Mt. Etna related to dike injection leading to the 2001 and 2002-2003 flank eruptions, *EGU Conference, Vienna, Austria, April 2006*.

Barberi, G., Cocina, O., Maiolino, V., Musumeci, C., Privitera E., 2004. Insight into Mt. Etna (Italy) kinematics during 2002-2003 eruption as inferred by seismic stress and strain tensors inversion, *Geophys. Res. Lett.*, **31**, L2164, doi:10.1029/2004GL020918.

Boatwright, J., 1984. The effect of rupture complexity in estimate of source size, *J. Geophys. Res.*, 89, 1132–1146.

Bonaccorso, A., Ferrucci, F., Patanè, D., Villari L., 1996. Fast deformation processes and eruptive activity at Mt. Etna (Italy). J. *Geophys. Res.*, **101**, B8, 17467-17480.

Cocina, O., Neri, G., Privitera, E., Spampinato S., 1997. Stress tensor computations in the Mount Etna area (Southern Italy) and tectonic implications. *J. Geodynamics*, **23**, 2, 109-127.

Cramér, H., 1946, *Mathematical Methods of Statistics*, Princeton Mathematical Series, (M. Morse and W. Tucker, eds). Princeton University Press, Princeton, USA.

D'Amico, S. and Maiolino, V. 2005. Local magnitude estimate at Mt. Etna, *Ann. Geophys*., **48**, 215-229.

Deichmann, N., 1997. Far field pulse shapes from circular sources with variable rupture velocities, *Bull. seism. Soc. Am.,* **87,** 1288–1296.

de Lorenzo, S. and Zollo, A., 2003. Size and geometry of microearthquake seismic ruptures from *P* and *S* Pulse Width Data, *Geophys. J. Int.*, **155**, 422–442.

de Lorenzo, S., Di Grazia, G., Giampiccolo, E., Gresta, S., Langer, H.,Tusa, G., Ursino, A.,,2004. Source and Qp parameters from pulse width inversion of microearthquake data in southeastern Sicily, Italy, *J. Geophys. Res.,* **109**, B07308, doi:10.1029/2003JB002577.

de Lorenzo, S., Filippucci, M., Giampiccolo, E., Patanè, D., 2006. Intrinsic *Qp* at Mt. Etna from the inversion of rise times of 2002 microearthquake sequence, *Ann. Geophys*, **49**, 1215-1234.

Evans, J.R., Eberhart-Phillips, D., Thurber, C.H., 1994. Users's manual for SIMULPS12 for imaging Vp and Vp/Vs:a derivative of the Thurber tomographic inversion SIMUL3 for local earthquakes and explosions, *US Geol. Survey, Open File Report*, 94-431

Filippucci, M., de Lorenzo, S., Boschi, E., 2006, Fault plane orientations of small earthquakes of the 1997 Umbria-Marche (Italy) seismic sequence from P-wave polarities and rise times, *Geophys. J. Int.,* **166**(1), 322– 338, doi:10.1111/j.1365-246X.2006.02998.x.

Giampiccolo, E., D'Amico, S., Patanè, D., Gresta, S., 2007. Attenuation and source parameters of shallow microearthquakes at Mt. Etna volcano (Italy), *Bull. Seism. Soc. Am.*, **97**, 1B, 184-197.

Gresta, S., Peruzza, L., Slejko, D., Di Stefano, G.,, 1998. Inferences on the main volcano-tectonic structures at Mt. Etna (Sicily) from a probabilistic seismological approach, *J. Seismology*, **2**, 105-116.

Keilis-Borok, V.I. (1959): On estimation of the displacement in an earthquake source dimensions, *Ann. Geofis.*, **XII**, 205-214.

Lanzafame, G. Neri, M., Rust, D., 1996. A preliminary structural evaluation of recent tectonic activity on the eastern flank of Mount Etna, Sicily, *West London Pap. Environ. Stud*., **3**, 73–90.

Mori, J., 1996. Rupture directivity and slip distribution of theM4.3 foreshock to the 1992 Joshua Tree earthquake, Southern California, *Bull. seism. Soc.Am.,* **86,** 805–810

Musumeci, C., Cocina, O., De Gori, P., Patanè, D., 2004. Seismological evidences of stress induced by dike injection during the 2001 Mt. Etna eruption, *Geophys. Res. Lett*., **31**, L07617, doi:10.1029/2003GL019367.

Patanè, D., Privitera, E., 2001. Seismicity related to 1989 and 1991-93 Mt. Etna (Italy) eruptions: kinematic constraints by fault solution analysis. *J. Volcanol. Geotherm. Res.*, **109**, 77 – 98.

Patane`, D., Barberi, G., Cocina, O., De Gori, P., Chiarabba, C., 2006. Time-Resolved Seismic Tomography Detects Magma Intrusions at Mount Etna, *Science*, **313**, 821-823.

Patanè, D., Giampiccolo, E., 2004. Faulting Processes and Earthquake Source Parameters at Mount Etna: State of the Art and Perspectives. In: *Etna Volcano Laboratory*, (A. Bonaccorso, S. Calvari, M. Coltelli, C. Del Negro and S. Falsaperla, eds). AGU (Geophysical monograph series), 167-189.

Press,W.H., Flannery, B.P., Teukolsky, S.A., Vetterling,W.T.,1989. *Numerical Recipes, The Art of Scientific Computing (Fortran Version),* Cambridge University Press, Cambridge, USA.

Rasà R., Ferrucci F., Gresta S., Patanè D.,1995. Etna: sistema di alimentazione profondo, assetto geostatico locale e bimodalità di funzionamento del vulcano. In: *Progetto Etna 1993-1995* (F. Ferrucci and F. Innocenti, eds). Pubblicazione Speciale GNV, 145-150.

Reasenberg, P., Oppheneimer, D.H., 1985. FPFIT, FPPLOT and FPPAGE: FORTRAN computer program for calculating and displaying earthquake fault-plane solutions, *US Geological Survey Report*, 85–739.

Tanguy, J. C., Condomines, C. and Kieffer, G. 1997, Evolution of the Mount Etna magma: constraints on the present feeding system and eruptive mechanisms, *J. Volcanol. Geoth. Res*., **75**, 221-250

Vasco, D.W. and Johnson, L.R., 1998. Whole earth structure estimated from seismic arrival times, *J. Geophys. Res.*, **103**, 2633–2672.

Warren, L.M. & Shearer, P.M., 2006. Systematic determination of earthquake rupture directivity and fault planes from analysis of long-period *P*-wave spectra, *Geophys., J. Int.,* **164,** 46–62.

Zollo, A., de Lorenzo, S., 2001. Source parameters and three-dimensional attenuation structure from the inversion of microearthquake pulse width data: Method and synthetic tests, *J. Geophys. Res.*, **106**, 16,287– 16,306.